Materials Science and Engineering C 53 (2015) 43–49

Contents lists available at ScienceDirect

Materials Science and Engineering C

journal homepage: www.elsevier.com/locate/msec

A novel nitrite biosensor based on the direct electron transfer hemoglobin immobilized in the WO_3 nanowires with high length–diameter ratio

Hui Liu *, Congyue Duan, Chenhui Yang, Xianjin Chen, Wanqiu Shen, Zhenfeng Zhu

School of Materials Science and Engineering, Shaanxi University of Science and Technology, Xi'an 710021, PR China

ARTICLE INFO

Article history:
Received 4 February 2015
Received in revised form 27 March 2015
Accepted 10 April 2015
Available online 15 April 2015

Keywords:
Biosensor
WO_3
Nanowires with high length–diameter ratio
Direct electron transfer (DET)
Nitrite

ABSTRACT

WO_3 nanowires (WO_3NWs) with high length–diameter ratio have been synthesized through a simple synthetic route without any additive and then used to immobilize hemoglobin (Hb) to fabricate a mediator-free biosensor. The morphology and structure of WO_3NWs were characterized by scanning electron microscopy, transmission electronic microscopy and X-ray diffraction. Spectroscopic and electrochemical results revealed that WO_3NWs are an excellent immobilization matrix with biocompatibility for redox protein, affording good protein bioactivity and stability. Meanwhile, due to unique morphology and property of the WO_3 nanowires, the direct electron transfer of Hb is facilitated and the prepared biosensors displayed good performance for the detection of nitrite with a wide linear range of 1 to 4200 μM, as well as an extremely low detection limit of 0.28 μM. The WO_3 nanowires with high length–diameter ratio could be a promising matrix for the fabrication of mediator-free biosensors, and may find wide potential applications in environmental analysis and biomedical detection.

1. Introduction

The studies of direct electron transfer (DET) of redox proteins or enzymes not only can help to understand the intrinsic thermodynamic and kinetic properties of proteins, but also establish a foundation for fabricating mediator-free biosensor [1,2]. However, due to the deep burying of electroactive center in the protein structure and the denaturation of proteins on the bare electrode surface, it is difficult for proteins to realize the DET process on the bare electrode [3,4]. Recent researches show that a series of nanomaterials with special quantum size effect and surface effect can be used to immobilize enzymes, facilitate the direct electron transfer and fabricate mediator-free biosensors [4,5]. Among them, metal oxide nanowires, such as SnO_2 [6], CuO [7], TiO_2 [8], and MnO_2 [9], have received increasing attention due to their unique electrical property that nanowires have direct one-dimensional electronic pathway, facilitating the charge transport [6,9]. However, to the best of our knowledge, WO_3 nanowires with relatively high conductivity as well as non-toxicity for constructing direct electrochemical biosensor have rarely been reported [10].

Here, WO_3 nanowires (WO_3NWs) with high length–diameter ratio were synthesized by a simple hydrothermal process followed by calcinations. The WO_3NWs with high length–diameter ratio possess many advantages as the electrode materials. As shown in Scheme 1, this kind of long nanowires could form a tightly woven piece of net on the electrode for enzyme immobilization. Due to the relatively smaller diameter (diameter less than 20 nm), the specific surface area of WO_3NW is large, which is beneficial to adsorbing enzymes, especially electrostatic adsorption. Meanwhile, the space among nanowires is a route of the diffusion of electrolyte containing substrate. So the substrate can simply get into the net of WO_3NWs and has access to the enzymes immobilized in the net. WO_3NWs with relatively high mobility of charge carriers can also become the good media of efficient electrical communication between the enzyme and the electrode. Hence, such kind of WO_3NWs should be a promising support for enzyme immobilization and has potential applications in biosensors.

In this work, hemoglobin (Hb) was selected as a model redox protein for construction of the biosensor. The performance of a sensor composed of Hb immobilized in the WO_3NWs was compared with that of sensors based on WO_3 nanosheets, in order to highlight the advantages of the WO_3NWs as a support.

2. Experimental

2.1. Materials and apparatus

Hb (from bovine blood) and Nafion solution (5 wt.% in lower aliphatic alcohols) were purchased from Sigma. Unless otherwise noted, all other chemicals (analytical grade) were purchased from Sinopharm Chemical Reagent Co., Ltd., China. In all experiments, deionized water was used.

* Corresponding author.
E-mail address: liuhui@sust.edu.cn (H. Liu).

http://dx.doi.org/10.1016/j.msec.2015.04.016
0928-4931/

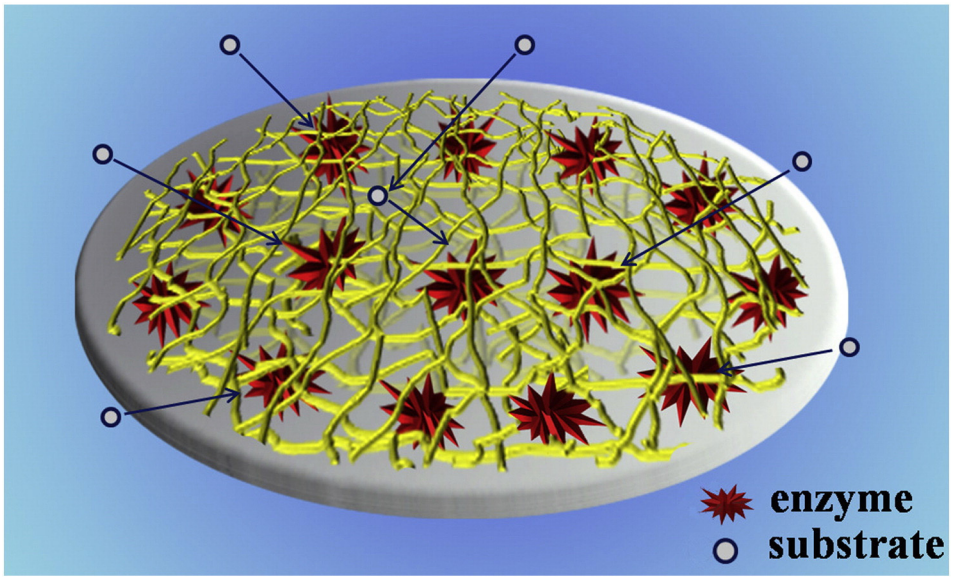

Scheme 1. Schematic illustration of the WO_3NWs immobilizing hemoglobin.

Field-emission scanning electron microscopy (FE-SEM) was performed using a Hitachi S-4800 & Hiroba energy dispersive X-ray electron microscope. Transmission electronic microscopy (TEM) images were obtained on a Hitachi H-800 instrument. X-ray diffraction (XRD) patterns were recorded on a Rigaku D/max 2200pc diffractometer using Cu Kα radiation of wavelength $\lambda = 0.15418$ nm at 40 kV and 40 mA. FT-IR spectra were obtained on a Bruker TENSOR27 instrument. UV–vis spectra were recorded using a PerkinElmer Lambda-950 spectrophotometer. All electrochemical experiments were performed with a CHI 660D electrochemical workstation (CH Instruments, Shanghai, China). A conventional three-electrode system, which consisted of a platinum wire as the counter electrode, an Ag/AgCl/3 M KCl as the reference electrode and a 3-mm diameter modified glassy carbon electrode (GCE) as the working electrode, was used in all electrochemical experiments. Unless otherwise noted, 0.1 M phosphate buffered saline (PBS; pH 7.0) was used as the supporting electrolyte in all experiments. The buffer was purged with highly purified nitrogen for at least 30 min and a nitrogen atmosphere environment was kept in electrochemical measurements.

2.2. Preparation of WO_3 nanowires

In a typical synthesis, 0.1 g of WCl_6 was added into 100 mL of absolute ethanol, and a clear yellow solution was formed immediately (Fig. S1A). After stirring for 60 min, the solution became a clear cyan solution (Fig. S1B). The clear cyan solution was then loaded into a Teflon-lined autoclave. The autoclave was sealed, heated in an oven of 180 °C for 24 h, and was then allowed to cool to room temperature. A blue floccule product (precursor of $WO_{2.72}$) was collected by centrifugation and rinsed sequentially with ethanol and water for several times, and then dried at 50 °C for 5 h. The blue product was heated to 450 °C at a rate of 1 °C/min, and then annealed at 450 °C for 30 min. The final yellow product (WO_3NWs) was formed.

2.3. Preparation of enzyme electrode

Prior to use, the glassy carbon electrode (GCE) was sequentially polished using 1.0, 0.3 and 0.05 μm alumina powder on a polishing cloth and rinsing with deionized water in between. The electrode was then sonicated in ethanol and deionized water. Next, the electrode was dried using a purified nitrogen stream. The enzyme electrode was prepared by a simple casting method. Firstly, 2 mg mL^{-1} WO_3NW suspension was obtained by adding 10 mg of as-prepared WO_3NWs into 5 mL water with the aid of ultrasonication and stirring. Then, a suspension (denoted as Suspension I), which contained a final concentration of 2.5 mg mL^{-1} Hb and 1 mg mL^{-1} WO_3NWs, was prepared by mixing appropriate volume of Hb solution (10 mg mL^{-1}, dissolved in 0.1 M pH 7.0 PBS) and WO_3NW suspension (2 mg mL^{-1}) thoroughly. Finally, 4 μL of Suspension I was applied to the surface of a freshly polished GCE to prepare the WO_3NWs/Hb/GCE. A beaker was covered over the electrode so that water can evaporate slowly in air and a uniform film electrode can be obtained. The dried WO_3NWs/Hb/GCE was stored at 4 °C in refrigerator when not in use.

For comparison, WO_3 nanosheets (WO_3NSs) were used for the fabrication of WO_3NSs/Hb/GCE with similar procedures as described above. Fig. S2 and Fig. S3 give the SEM images and XRD patterns of the WO_3NSs. In the control experiment, Nafion/Hb/GCE and WO_3NSs/GCE were also prepared. It should be noted that the protein load on the surface of different modified electrodes (except the WO_3NSs/GCE) was equal. Before electrochemical measurements, all the as-prepared film electrodes were immersed in pH 7.0 PBS for 30 min to remove residual components.

3. Results and discussion

3.1. Characterization of WO_3 nanowires

Fig. 1 presents the XRD patterns of the precursor (a) and WO_3NWs (b). As can be seen, before calcinations, the diffraction patterns of precursors correspond to standard $WO_{2.72}$ (JCPDS No. 36-101) [11]. After annealed at 450 °C the precursors were thoroughly converted into pure WO_3 (JCPDS No. 43-1035).

Fig. 2 shows typical SEM and TEM images of the samples prepared at various stages. From Fig. 2A, it is observed that $WO_{2.72}$ shows relatively uniform nanowire morphology with diameters less than 20 nm and lengths longer than 5 μm. The inset of Fig. 2A presents the high-resolution TEM (HRTEM) image. The spacing between adjacent lattice planes is 0.37 nm, corresponding to the (010) planes of monoclinic $WO_{2.72}$, which indicates that the preferential growth direction is [010]. Fig. 2B and C indicates that calcinations at 450 °C for 30 min did not change the morphology of nanowires, which may be attributed to the mild calcination temperature, slow heating rate (1 °C/min), and the similar crystal structure between WO_3 and $WO_{2.79}$ [12]. The HRTEM image (Fig. 2D) further confirms the single-crystalline nature of the

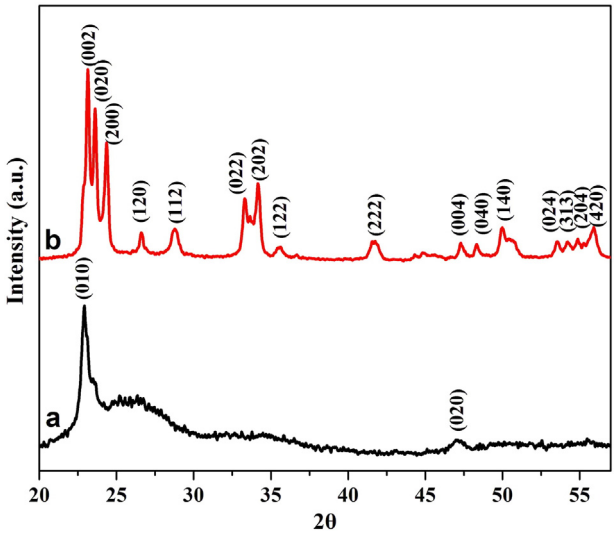

Fig. 1. XRD of precursors (a) and WO_3 nanowires (b).

WO_3 nanowires. The fringe spacing of 0.38 and 0.37 nm agrees well with the spacing of the (200) and (002) lattice planes of WO_3.

3.2. Encapsulation of Hb in the WO_3 nanowires

Fig. 3A gives the image of WO_3NWs/Hb/GCE. As can be seen, WO_3NWs with large length–diameter ratio could form a tightly woven piece of net on GCE which owns numerous interspaces among WO_3NWs. The interspaces are available for Hb entrapment. Furthermore, the nanoscale WO_3 wires (less than 20 nm in diameter) can greatly enhance the active surface area available for protein binding.

The stability of Hb immobilized on WO_3NWs/GCE was investigated by UV–vis spectroscopy [13–15]. The Soret absorption bands of heme proteins provide information about the conformational integrity of the proteins. As shown in Fig. 3B, the Soret absorption band of Hb immobilized on WO_3NWs/GCE (storage at 4 °C for four weeks) is located at 405.3 nm (curve a), which is close to that of native Hb at 406.2 nm (curve b), indicating that Hb retained the essential features of its conformational integrity. This reveals that WO_3NWs have biocompatibility and did not suffer significant protein denaturation.

FTIR spectroscopy is also an effective means to explore the secondary structure of Hb entrapped in WO_3NWs/GCE [14–17]. The shapes of amide I and amide II bands of protein provide detailed information on the secondary structure of polypeptide chain [18]. As shown by the FTIR spectrum of Hb (curve a) in Fig. S4, the amide I band (1700–1600 cm^{-1}) results from C═O stretching vibration of peptide linkages in the backbone of protein. The amide II band (1620–1500 cm^{-1}) is caused by the combination of N–H bending and C–N stretching. As shown in Fig. S4, the spectrum of amide I and II bands of Hb in WO_3NWs/Hb composite film (1658 and 1540 cm^{-1}, Fig. S4A) is almost the same as that obtained for native Hb (1657 and 1539 cm^{-1}, Fig. S4B), and is essentially consistent with the reported value of native Hb [15,17,19]. The similarities of the two spectra demonstrated that Hb retained the essential features of its native secondary structure on WO_3NWs/GCE. This WO_3NW with good biocompatibility will be a promising matrix for protein immobilization and biosensor fabrication.

3.3. Direct electrochemistry behavior of WO_3NWs/Hb/GCE

Fig. 4 depicts the typical cyclic voltammograms (CVs) of different modified electrodes in 0.1 M PBS (pH 7.0) at a scan rate of 0.1 V s^{-1}. No redox peak is observed at WO_3NWs/GCE (curve a), which indicates that WO_3NWs/GCE is electroinactive in the potential window. The WO_3NWs/Hb/GCE (curve d) exhibits a couple of stable and well-defined redox peaks at −0.369 V and −0.327 V vs. Ag/AgCl, which could be ascribed to direct electron transfer between Hb and the underlying electrode. According to Lu et al. [16], the electron transfer of Hb occurs between the Fe^{III} and Fe^{II} site within Hb. The formal potential ($E^{0'} = (E_{p,a} + E_{p,c}) / 2$) of Hb was −0.348 V vs. Ag/AgCl is in agreement with −0.345 V, −0.353 V and −0.36 V vs. Ag/AgCl reported for the Hb($Fe^{III/II}$) redox couple in Hb-ZnO-Nafion, Hb-ZnO-MCNT-Nafion and Hb-CNF-Nafion films [16,19,20]. The potential difference (ΔE_p) between the anodic and cathodic peak potential is about 42 mV. Such a small ΔE_p

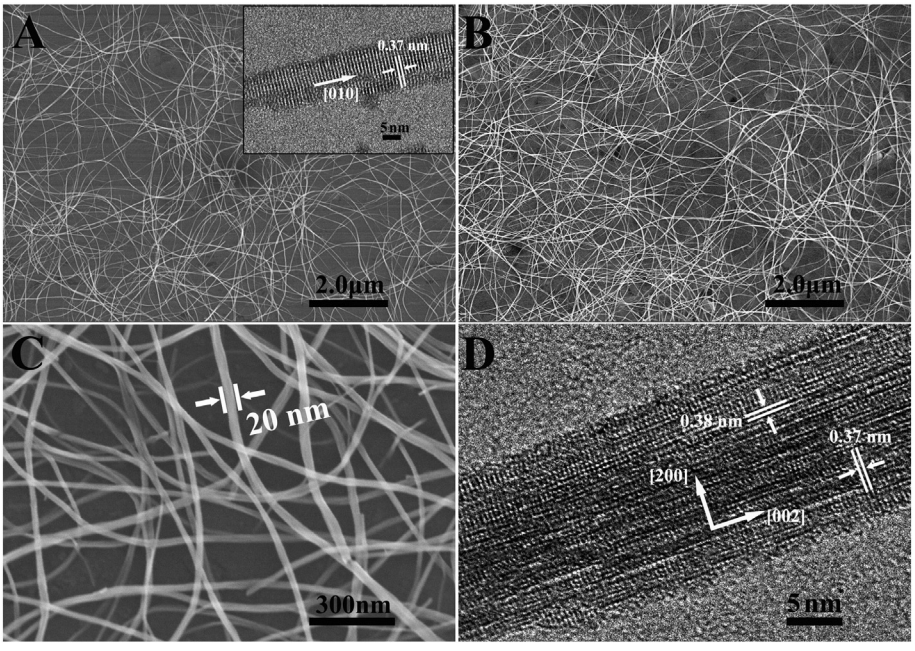

Fig. 2. SEM and TEM images. (A) Typical SEM micrographs of the $WO_{2.72}$ nanowires; the inset is the HRTEM image of the sample. (B and C) Low- and high-magnification SEM images of the WO_3 nanowires. (D) HRTEM image of the WO_3 nanowires.

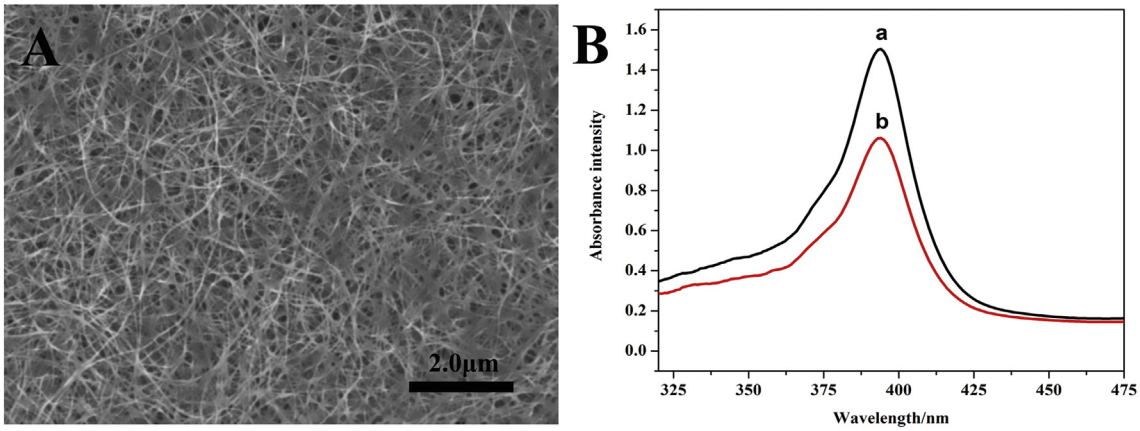

Fig. 3. (A) Typical SEM image of WO_3NWs/Hb composite film and (B) UV–vis spectra of WO_3NWs/Hb composite film (storing at 4 °C for 21 days) (a) and Hb (b).

value reveals a fast and quasi-reversible electron-transfer process, revealing that the WO_3 nanowires can provide a favorable microenvironment for Hb to undergo a facile electron-transfer reaction. Compared with that of the WO_3NWs/Hb/GCE, almost no redox peaks observed at the Nafion/Hb/GCE (curve b, in Fig. 4), suggesting an enhanced electron transfer between Hb molecules and the surface of the WO_3NWs/Hb/GCE. Meanwhile, due to the deep burying of electroactive center in the protein structure and the denaturation of proteins on the bare electrode surface, it is difficult for proteins to realize the DET process on the bare electrode [3,5]. It can be clearly seen from the comparison that direct electron transfer between Hb molecules and GCE is greatly enhanced at the WO_3NWs/Hb/GCE. For comparison, WO_3NSs/Hb/GCE has also been carried out (curve c, in Fig. 4). The redox peaks of the electrode are 53.8% smaller than that of WO_3NWs/Hb/GCE. The ΔE_p is 53 mV, which is larger than that of WO_3NWs/Hb/GCE (42 mV), indicating slower electron transfer rate of Hb on the electrode than on WO_3NSs/Hb/GCE. It can be concluded that WO_3 nanowires have better effect on the facilitation of electron transfer, which may result from unique morphology and property of the WO_3 nanowires.

Fig. 5 shows the cyclic voltammograms of 0.1 M PBS (pH 7.0) at a WO_3NWs/Hb/GCE when the scan rate was increased from 0.1 to 0.8 V s^{-1}. With the increase of the scan rate, the cathodic and anodic peak currents of Hb increase simultaneously, meanwhile the cathodic and anodic peak potentials show a small shift and the peak to peak separation also become slightly enlarged. The inset of Fig. 5 shows that the cathodic (i_{pc}) and anodic (i_{pa}) peak currents increase linearly with scan rates from 0.1 to 0.8 V s^{-1}. This reveals that the electrode reaction corresponds to a surface-controlled quasi-reversible process. Using the Laviron method for a surface-controlled electrochemical system [21], the apparent heterogeneous electron transfer rate constant (k_s) of Hb immobilized on WO_3NWs/Hb/GCE is estimated to be about 3.1 s^{-1}, which is higher than the value reported for Hb immobilized TiO_2 nanorods-graphene (0.65 s^{-1}) [15], AuNPs/ZnO/Gr nanocomposite (1.3 s^{-1}) [22] flower-like NiO microspheres (2.54 s^{-1}) [5], suggesting a faster electron-transfer process. This means that the WO_3 nanowires facilitate the direct electron transfer of Hb.

The average surface concentration of electroactive Hb (Γ^*, mol cm^{-2}) can be estimated from the charge integration of the reduction peak of the CV using the formula:

$$Q = nFA\Gamma* \quad (1)$$

where F is Faraday constant, Q is the charge (C) and can be obtained by integrating the reduction peak of Hb, n and A stand for the number of electron transferred and the geometrical surface area of the electrode, respectively. According to this method, the surface concentration of electroactive Hb (Γ^*) at WO_3NWs/Hb/GCE was calculated as 1.36×10^{-10} mol cm^{-2}, which is much greater than the theoretical value for monolayer coverage (1.89×10^{-11} mol cm^{-2}) [23]. This means that multilayers of Hb entrapped in the WO_3NWs/Hb/GCE participated in the electron-transfer process.

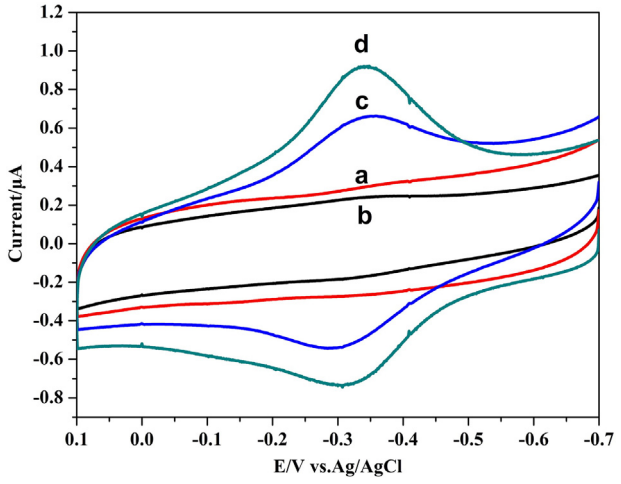

Fig. 4. Cyclic voltammograms of the WO_3NWs/GCE (a), Nafion/Hb/GCE (b), WO_3NSs/Hb/GCE (c), and WO_3NWs/Hb/GCE (d), in 0.1 M pH 7.0 PBS with a scan rate of 0.1 V s^{-1}.

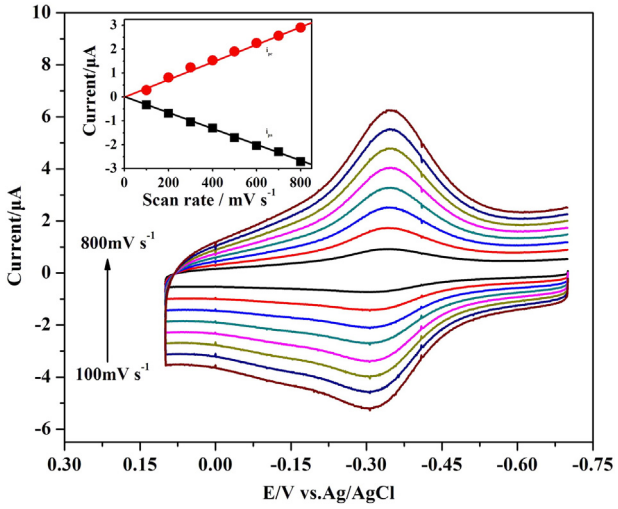

Fig. 5. Cyclic voltammograms of the Nafion/Hb/WO_3NWs/GCE in 0.1 M pH 7.0 PBS with increasing scan rates from 0.1 to 0.8 V s^{-1}. Inset: plot of cathodic and anodic peak current vs. scan rate.

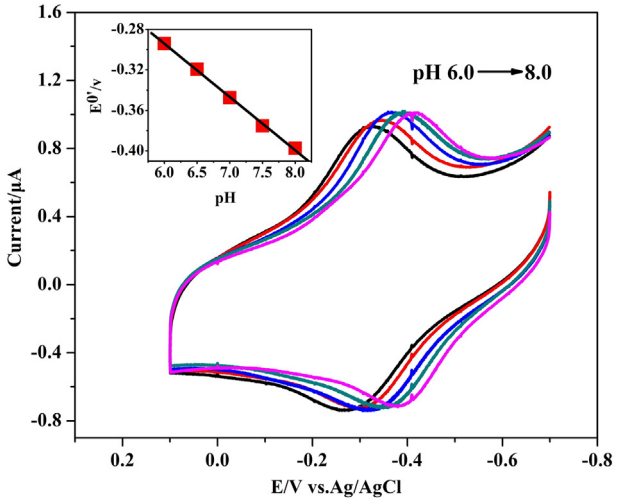

Fig. 6. Cyclic voltammograms of the WO_3NWs/Hb/GCE in 0.1 M pH 7.0 PBS with increasing scan rates from 0.1 to 0.8 V s^{-1}. Inset: plot of cathodic and anodic peak current vs. scan rate.

Fig. 6 shows the cyclic voltammograms of 0.1 M PBS of different pH values at a WO_3NWs/Hb/GCE. Stable and well-defined CVs were observed in the pH range 6.0–8.0. With the increase of pH value, both the cathodic and anodic peaks shifted to the negative (Fig. 6). This can be contributed to the involvement of proton transfer in the Hb(Fe^{III})/Hb(Fe^{II}) redox couple [24]. The $E^{0'}$ value of Hb varied linearly in the range of pH 6.0–8.0, with a slop of −52.9 mV pH^{-1} (the inset of Fig. 6). This value is very close to the theoretical value for the transfer of one proton and electron in a reversible reduction (−58 mV pH^{-1} at 25 °C) [24,25].

3.4. Electrocatalysis of WO_3NWs/Hb/GCE to reduction of nitrite

In order to study the electrocatalytic activity of Hb immobilized in WO_3NWs/Hb/GCE, its response to the reduction of nitrite was explored. Fig. 7A showed the CVs of WO_3NWs/Hb/GCE in 0.1 M PBS (pH 5.5) containing different concentrations of $NaNO_2$. Only a couple of stable and well-defined redox peaks at −0.292 V and −0.237 V vs. Ag/AgCl, which could be ascribed to direct electron transfer between Hb and the underlying electrode, is observed for WO_3NWs/Hb/GCE in PBS without $NaNO_2$. Upon addition of $NaNO_2$, a new irreversible reduction peak located at −0.710 V is observed, and the peak current increased linearly with the increase of $NaNO_2$ concentration. In contrast, no significant reduction peak of $NaNO_2$ was observed on WO_3NWs/GCE (the inset of Fig. 7A), which indicated that the irreversible reduction wave was not a result of the WO_3NWs.

The reduction product at −0.710 V is most likely N_2O, and the mechanism of the electrocatalytic reduction of nitrite at Hb-based electrode can be proposed as follows [26,27]:

$$\mathrm{Hb}\left(\mathrm{Fe^{III}}\right) + \mathrm{e^-} \rightleftarrows \mathrm{Hb}\left(\mathrm{Fe^{II}}\right) \quad (2)$$

$$\mathrm{Hb}\left(\mathrm{Fe^{II}}\right) + \mathrm{HNO_2} + \mathrm{H^+} \rightarrow \left[\mathrm{Hb}\left(\mathrm{Fe^{II}}\right)-\mathrm{NO}\right]^+ + \mathrm{H_2O} \quad (3)$$

$$\left[\mathrm{Hb}\left(\mathrm{Fe^{II}}\right)-\mathrm{NO}\right]^+ + \mathrm{e^-} \rightarrow \left[\mathrm{Hb}\left(\mathrm{Fe^{II}}\right)-\mathrm{NO}\right]^{\cdot} \quad (4)$$

$$\left[\mathrm{Hb}\left(\mathrm{Fe^{II}}\right)-\mathrm{NO}\right]^{\cdot} + \mathrm{e^-} \rightarrow \left[\mathrm{Hb}\left(\mathrm{Fe^{II}}\right)-\mathrm{NO}\right]^- \quad (5)$$

$$\left[\mathrm{Hb}\left(\mathrm{Fe^{II}}\right)-\mathrm{NO}\right]^- + \mathrm{H^+} \rightarrow \mathrm{Hb}\left(\mathrm{Fe^{II}}\right) + \mathrm{HNO} \quad (6)$$

$$2\mathrm{HNO} \rightarrow \mathrm{N_2O} + \mathrm{H_2O}. \quad (7)$$

Obviously, the acidity of the detection solution has a significant effect on the catalytic reduction of $NaNO_2$ because the catalysis of Hb to $NaNO_2$ is accompanied by the transfer of protons. Therefore, the effect of the buffer solution pH value on the biosensor response in the presence of 500 μM $NaNO_2$ is studied (Fig. 7B). Both the peak potential and current are depended on pH value. With the decrease of pH value, the peak potential shifted positively suggesting a proton-coupled reaction [28]. It is clearly seen from Fig. 7B that the peak current increased with the value of pH from 7.0 to 5.5, this may be attributed that, as a reactant of the electrocatalytic reduction reaction, the increasing concentration of H^+ could facilitate electrocatalytic reduction of nitrite at Hb-based electrode (Eqs. (3)–(7)). While the peak current drops down from pH 5.5 to 4.0, this may be caused by denaturation of Hb that existed to a considerable extent (This can be proved by the UV–vis absorbance spectra of Hb in different pH buffer solutions. Fig. S5) when the pH shifted toward a more acidic direction. It is obviously that this biosensor has the optimum sensitivity at pH 5.5 for the detection of $NaNO_2$. Meanwhile, these results suggest that the catalytic reduction of $NaNO_2$ depends on not only the acidity of the detection solution but also the bioactivity of Hb.

3.5. Biosensor performance of the WO_3NWs/Hb/GCE

As is well known, nitrite is a toxicant which widely exists in polluted water and antiseptic food. It is vitally important to detect nitrite in the

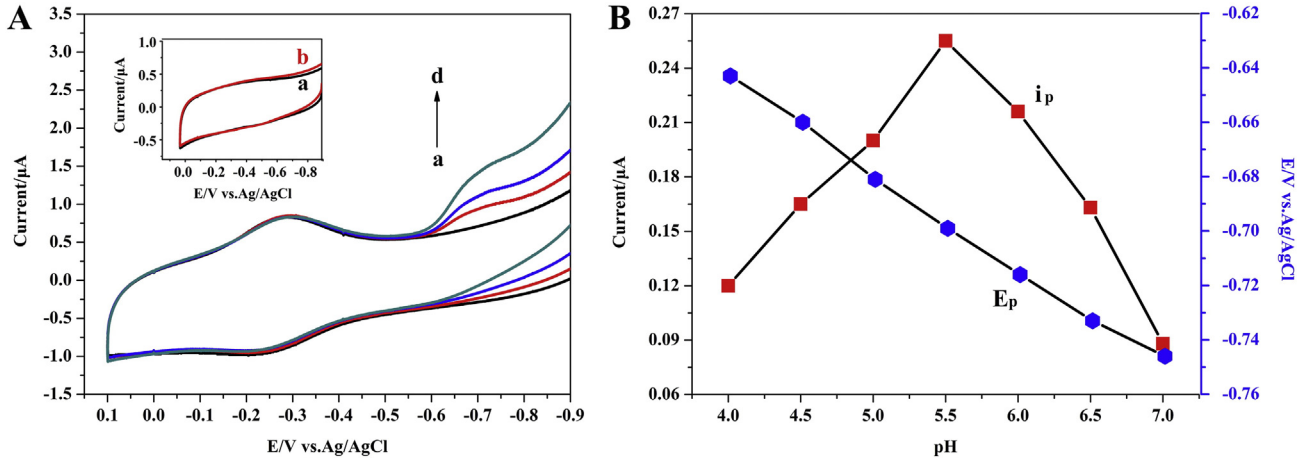

Fig. 7. (A) Cyclic voltammograms of the WO_3NWs/Hb/GCE in 0.1 M pH 5.5 PBS containing 0 (a), 200 (b), 400 (c), and 700 (d), $NaNO_2$ with a scan rate of 0.1 V s^{-1}; the inset: cyclic voltammograms of the WO_3NWs/GCE in 0.1 M pH 5.5 PBS containing 0 (a) and 400 (b). (B) Variations of catalytic currents and peak potentials vs. pH of WO_3NWs/Hb/GCE.

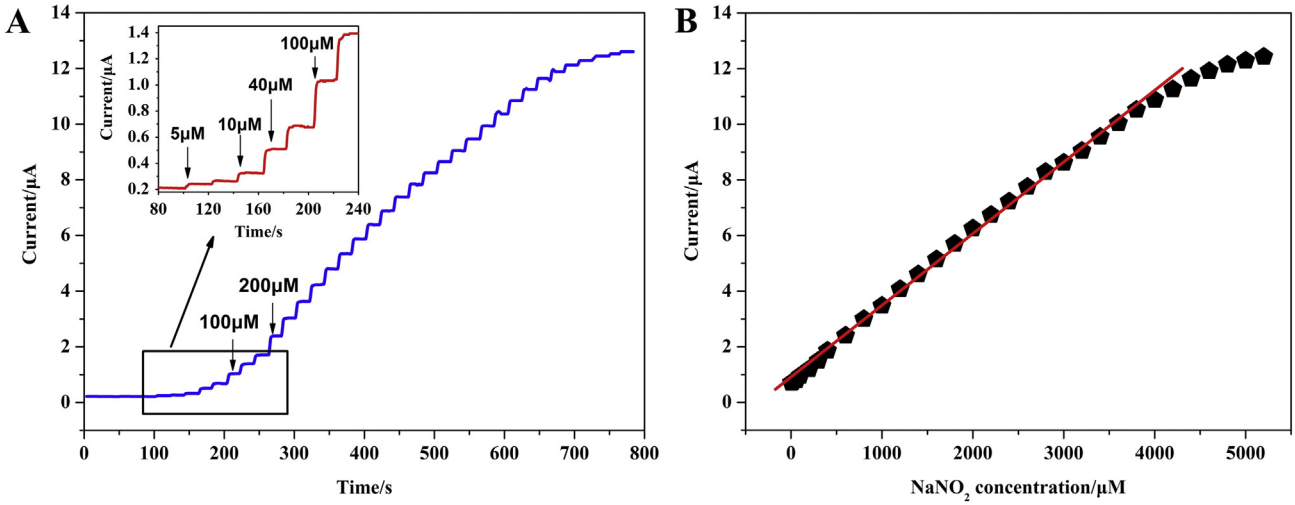

Fig. 8. (A) Typical current–time response of the Nafion/Hb/WO_3NWs/GCE at −0.70 V to successive addition of $NaNO_2$ in stirred 0.1 M pH 5.5 PBS. (B) Plot of steady state current vs. $NaNO_2$ concentration.

fields of biological and environmental chemistry. The biosensor performance for the detection of nitrite of the WO_3NWs/Hb/GCE was also investigated by amperometry. Fig. 8 gives the amperometric responses of WO_3NWs/Hb/GCE at −0.70 V after adding $NaNO_2$ in stirred PBS (1.0 M, pH 5.5). Fig. 8A demonstrates that the response time (achieving 95% of the steady-state current) was less than 3 s. Moreover, a well-defined linear relationship between the current and the $NaNO_2$ concentration was observed. The calibration plot (Fig. 8B) showed a linear range from 1 to 4200 μM with a correlation coefficient of 0.9988 (N = 27). The detection limit was estimated to be 0.28 μM (based on a signal-to-noise ratio of 3). Performances of various nitrite biosensors are listed in Table S1. It is clear that the performance of WO_3NWs/Hb/GCE was significantly improved. Furthermore, compared with WO_3 nanosheets, the WO_3NW based biosensor has better performance (Fig. S6 and Table S2). There are some reasons why the WO_3NWs/Hb/GCE displays both a lower detection limit and a wider linear range. Firstly, WO_3 nanowires could provide a favorable microenvironment for the protein to retain its stability. More importantly, the space among nanowires is a route of the diffusion of electrolyte containing substrate. So the substrate can simply get into the net of WO_3NWs and has access to the enzymes immobilized in the net. Furthermore, WO_3NWs with relatively high mobility of charge carriers can also become the good media of efficient electrical communication between the protein and the electrode.

3.6. Stability and reproducibility of the biosensor

Cycle stability is an important evaluation index for estimating the performance of biosensor. 100 continuous cyclic scans on WO_3NSs/Hb/GCE were repeated in the potential range from −0.7 to 0.1 V with a scan rate of 0.1 V s^{-1} (Fig. S7). No obvious change of CV curve could be observed. Hence, the prepared WO_3NSs/Hb/GCE possesses excellent cycle stability.

The long-term stability of fabricated biosensors was studied by examining its current response after storage at 4 °C. The biosensors could retain 93.7% of the initial response to $NaNO_2$ after four-week storage, demonstrating good long-term stability (Fig. S8). The good long-term stability can be contributed to the good biocompatibility of WO_3 nanowires, which can provide a favorable microenvironment for Hb to retain its bioactivity.

The reproducibility of the biosensor was investigated by determining 100 μM $NaNO_2$ in PBS (pH 5.5). The relative standard deviation (R.S.D.) was 2.9% for 5 successive measurements. Five biosensors prepared under the same conditions independently gave a R.S.D. of 3.4% for the determination of 100 μM $NaNO_2$ in PBS (pH 5.5), indicating an acceptable electrode-to-electrode reproducibility.

4. Conclusion

WO_3 nanowires with high length–diameter ratio have been synthesized through a simple synthetic route without any additive, and subsequently used to fabricate mediator-free biosensors for the detection of NO_2^-. The prepared mediator-free biosensors possess good performance for the detection for nitrite, with both a wide linear range of 1–4200 μM and a low detection limit of 0.28 μM (S/N = 3), as well as good stability and reproducibility. The improved performance of the biosensor can be attributed to unique morphology and property of the WO_3 nanowires. The WO_3 nanowires could not only form a tightly woven piece of net on the electrode to immobilize Hb, but also facilitate the direct electron transfer. Moreover, substrate can simply get into the net of WO_3 nanowires and has access to Hb immobilized in the net. This study indicates that WO_3 nanowires with high length–diameter ratio can be used as biocompatible matrix for the enzyme immobilization and the construction of direct electrochemical biosensor, and have great potential in environmental analysis.

Acknowledgments

This work was financially supported by the National Science Foundation of China (51272147), the Academic Backbone Cultivation Program of Shaanxi University of Science & Technology (XSGP201203) and the Graduate Innovation Found of Shaanxi University of Science and Technology.

Appendix A. Supplementary data

Supplementary data to this article can be found online at http://dx.doi.org/10.1016/j.msec.2015.04.016.

References

[1] I. Hamachi, A. Fujita, T. Kunitake, J. Am. Chem. Soc. 119 (1997) 9096–9102.
[2] W. Sun, L.L. Cao, Y. Deng, S.X. Gong, F. Shi, G.N. Li, Z.F. Sun, Anal. Chim. Acta 781 (2013) 41–47.
[3] Z.H. Zhu, L.N. Qu, Q.J. Niu, Y. Zeng, W. Sun, X.T. Huang, Biosens. Bioelectron. 26 (2011) 2119–2212.
[4] Q.L. Sheng, J.B. Zheng, X.D. Shangguan, W.H. Lin, Y.Y. Li, R.X. Liu, Electrochim. Acta 55 (2010) 3185–3191.
[5] S.Y. Dong, P.H. Zhang, H. Liu, N. Li, T.L. Huang, Biosens. Bioelectron. 26 (2011) 4082–4408.

[6] L.M. Li, J. Huang, T.H. Wang, H. Zhang, Y. Liu, J.H. Li, Biosens. Bioelectron. 25 (2010) 2436–2441.
[7] Y.M. Li, Q. Zhang, J.H. Li, Talanta 83 (2010) 162–166.
[8] C.C. Lin, Y.M. Chu, H.C. Chang, Sensors Actuators B 187 (2013) 533–539.
[9] L. Zhang, S.M. Yuan, L.M. Yang, Z. Fang, G.C. Zhao, Microchim. Acta 180 (2013) 627–633.
[10] H.D. Zheng, J.Z. Ou, M.S. Strano, R.B. Kaner, Adv. Funct. Mater. 21 (2011) 2175–2196.
[11] G.C. Xi, J.H. Ye, Q. Ma, N. Su, H. Bai, C. Wang, J. Am. Chem. Soc. 134 (2012) 6508–6511.
[12] G.C. Xi, B. Yue, J.Y. Cao, J.H. Ye, Chem. Eur. J. 17 (2011) 5145–5154.
[13] W. Sun, L.F. Dong, Y. Deng, J.H. Yu, W.C. Wang, Q.Q. Zhu, Mater. Sci. Eng. C 39 (2014) 86–91.
[14] W. Sun, S.X. Gong, F. Shi, L.L. Cao, L.Y. Ling, W.Z. Zheng, W.C. Wang, Mater. Sci. Eng. C 40 (2014) 235–241.
[15] W. Sun, Y.Q. Guo, X.M. Ju, Y.Y. Zhang, X.Z. Wang, Z.F. Sun, Biosens. Bioelectron. 42 (2013) 207–213.
[16] X.B. Lu, H.J. Zhang, Y.W. Ni, Q. Zhang, J.Q. Chen, Biosens. Bioelectron. 24 (2008) 93–98.
[17] Q.X. Ma, H. Wang, Y. Shu, X.W. Chen, J.H. Wang, RSC Adv. 4 (2014) 8177–8182.
[18] J.K. Kauppinen, D.J. Moffate, H.H. Mantsch, D.G. Lameron, Appl. Spectrosc. 35 (1981) 271–276.
[19] W. Ma, D.B. Tian, Bioelectrochemistry 78 (2010) 106–112.
[20] X.B. Lu, J.H. Zhou, W. Lu, Q. Liu, J.H. Li, Biosens. Bioelectron. 23 (2008) 1236–1243.
[21] E. Laviron, J. Electroanal. Chem. 101 (1979) 19–28.
[22] L.L. Xie, Y.D. Xu, X.Y. Cao, Colloids Surf. B 107 (2013) 245–250.
[23] S.F. Wang, T. Chen, Z.L. Zhang, X.C. Shen, Z.X. Lu, D.W. Pang, K.Y. Wong, Langmuir 21 (2005) 9260.
[24] X.Q. Chen, Q.X. Wang, L.H. Wang, F. Gao, W. Wang, Z.S. Hu, Biosens. Bioelectron. 66 (2015) 216–223.
[25] Q. Xie, Y.Y. Zhao, X. Chen, H.M. Liu, D.G. Evans, W.S. Yang, Biomaterials 32 (2011) 6588–6594.
[26] S. George, H.K. Lee, J. Phys. Chem. B 113 (2009) 15445–15454.
[27] M. ElKaoutita, A.H. Naggarb, I.N. Rodrigueza, J.H. Cisnerosa, Colloids Surf. B 92 (2012) 42–49.
[28] Y.X. Xu, C.G. Hu, S.S. Hu, Sensors Actuators B148 (2010) 253–258.